Since January 2020 Elsevier has created a COVID-19 resource centre with free information in English and Mandarin on the novel coronavirus COVID-19. The COVID-19 resource centre is hosted on Elsevier Connect, the company's public news and information website.

Available online at www.sciencedirect.com

ScienceDirect

Procedia Computer Science 192 (2021) 2095–2104

Procedia Computer Science

www.elsevier.com/locate/procedia

25th International Conference on Knowledge-Based and Intelligent Information & Engineering Systems

Immunization using a heterogeneous geo-spatial population model: A qualitative perspective on COVID-19 vaccination strategies

Alexandru Topîrceanu[a,*]

[a]*Department of Computer and Information Technology, Politehnica University Timisoara, Bd. V. Parvan 2, 300223 Timisoara, Romania*

Abstract

Epidemic modeling has been a key tool for understanding the impact of global viral outbreaks for over two decades. Recent developments of the COVID-19 pandemic have accelerated research using compartmental models, like SI, SIR, SEIR, with their appropriate modifications. However, there is a large body of recent research consolidated on homogeneous population mixing models, which are known to offer reduced tractability, and render conclusions hard to quantify. As such, based on our recent work, introducing the heterogeneous geo-spatial mobility population model (GPM), we adapt a modified SIR-V (susceptible–infected–recovered-vaccinated) epidemic model which embodies the idea of patient relapse from R back to S, vaccination of R and S patients (reducing their infectiousness), thus altering the infectiousness of V patients (from λ_n to λ_r). Simulation results spanning over a period of $t = 2000$ days (6 years, the period $\approx$ 2020–2025) compare the impact of an epidemic outbreak with variable vaccination strategies, starting after 1 year (as is the case of COVID-19). The infected proportion in the remaining 5-year period is analyzed using vaccination rates from $r_v = 0$ (no vaccination) to $r_v = 1$. While $r_v < 0.4$ is less effective during the earlier stages, all strategies with $r_v \geq 0.4$ show a similar downward convergence reducing the number of infected by more than half, compared to no vaccination. Given the complexity of epidemic processes, we conclude that higher vaccination rates yield similar results, but a minimal $r_v = 0.4$ (40% of population over five years) should be targeted.

Keywords: epidemic modeling; computational intelligence; heterogeneous population; geo-spatial mobility; vaccination strategies.

1. Introduction

Many recent studies in epidemic modeling are predominantly developing mass-action models into tools suitable for analyzing COVID-19 dynamics [9, 11, 4, 15, 18, 12]. Too often, nevertheless, these studies focus on customizing the underlying epidemic models (e.g., SIR, SEIR, SIRS), but consider homogeneous mixing of the population, implying that all individuals are fully connected inside a compartment or stochastic block [6, 27, 5, 4, 12]. Some studies propose

* Corresponding author. Tel.: +40-256-403261.
E-mail address: alext@cs.upt.ro

1877-0509
10.1016/j.procs.2021.08.217

so-called "flattening the curve" solutions that try to reduce the reproduction number R_0, but are also underpinned by homogeneous mixing models. Conversely, Watts *et al.* [36] found R_0 to have little influence on the predictability of large-scale epidemics, in the context of real-world, multi-scale population structures. Real-world population models are dictated by geographic, as well as historical, demographic and economic factors. As such, simplified population (and mobility) models, which lack the complexity of global scale population organization can lead to over- or under-estimations in terms of epidemic size and impact [8, 17, 12], or outbreak duration [4, 6, 18, 15].

Indeed, several state-of-the-art contributions developed increasingly realistic epidemic models by incorporating heterogeneous population mixing and human mobility patterns. Using Network Science, Salathé *et al.* [23] found that the topology of networks is a critical detail in explaining infectious dynamics, based on empirical data for viral diseases, e.g., SARS [20], HIV [3], measles [13], and influenza [12]. Furthermore, community structure has been observed to dictate the speed of epidemics. To this end, Shang *et al.* [25] study how overlapping communities and a higher network average degree accelerate infectious spreading. Salathé *et al.* [23] explain how the dynamics of epidemics over communities have implications on immunization strategies for large outbreaks. Chen *et al*. [7] show how overlapping in communities leads to increased infection rates and a higher spreading speed. Finally, we note the work of Stegehuis *et al*. [26] who demonstrate that the mesoscopic level of communities influences the behavior of percolation on networks, by stimulating or suppressing spreading speeds.

The main goal of this paper is to offer a qualitative forecast of vaccination strategies' efficacy, in the context of COVID-19. To this end, we employ epidemic modeling using an original heterogeneous population mixing model supported by geo-demographic data and daily estimations of COVID-19 cases. In our recent study [28], we introduce the geo-spatial mobility population model (GPM) which was compared to analogous homogeneous mixing models, and validated against real COVID-19 data [10]. Nevertheless, in [28], our research focus was on the community structure and individual mobility rather than on the transmission model; hence, a standard SIR epidemic model was incorporated into GPM to run numerical simulations. By contrast, this paper uses the underlying population mobility model of GPM and adapts a SIR-V (susceptible–infected–recovered–vaccinated) epidemic model with several considerations meant to increase the realism and the reliability of our analysis:

1. All recovered patients relapse back to susceptible after an average timeout of 3–6 months, as defined by recent studies [34, 14, 37]. Consequently, the recovered state is not a "final" state, as in the case of a classic SIR model.
2. All susceptible and recovered individuals can undergo vaccination defined by a constant rate r_v. During each simulation iteration, a constant proportion of random non-infected individuals are selected for vaccination.
3. Transmission to the vaccinated state will not render individuals immune to the epidemic. Conversely, as recent studies suggest [2], vaccinated individuals are less likely to get infected by roughly 75%. In other words, all vaccinated susceptible individuals are transformed back into susceptible individuals with a reduced infection probability λ_r, as opposed to non-vaccinated (normal) susceptibles with λ_n. Vaccinated recovered individuals keep their recovered state until the relapse timeout, when they become susceptibles with the reduced infection rate λ_r.

Given the increased realism of the GPM population model [28] and the proposed SIR-V epidemic model, inspired by recent scientific findings, we study the effect a variable vaccination rate r_v over a moderate time window (5 years). We reproduce a GPM model for several countries with different population densities, then analyze the dynamics of infected and recovered proportions using computer simulation.

2. Methods

2.1. The GPM model

Settlements are the basic form of human organization as they delimit the boundary between inhabited and non-inhabited land. To simplify our assumptions, the GPM model considers two levels of population organization, namely that of countries, and settlements (i.e., villages, towns, cities, regardless of region and size) inside each country. The current COVID-19 pandemic has shown that countries, even though an artificial political construct, are a highly

relevant form of population organization, as they can adopt different policies for population mobility (including lock-downs, social distancing, mobility restrictions) further influencing epidemic dynamics [33, 19].

The first ingredient of GPM is the generated realistic population structure. In essence, GPM translates into a two dimensional mesh of stochastic block models [16], with each block corresponding to a human settlement s_i (defined by a given country). Each settlement s_i is characterized by its real-world geographical position, using latitude (y) and longitude (x), and its size Ω_i (i.e., number of inhabitants). For higher accuracy, we use GPM at a country level, rather than a continental or global level, due to the sparsity of available data. All individuals from a settlement $n_j \in s_i$ are considered as interconnected, thus similar to a SIR compartmental model applied independently for each settlement. Nevertheless, the division of a total population into multiple (e.g., hundreds, thousands) of unique blocks is a significant factor favoring the realism of epidemic dynamics.

The second important ingredient of GPM is the modeled individual mobility. All individuals from a settlement s_i have the same probability of leaving to another settlement s_j. As such, we express the normalized probability of mobility from a settlement s_i to s_j as $p(s_i, s_j)$, given by the following equation:

$$p(s_i, s_j) = \frac{\Omega_j \cdot e^{-d_{ij}/\psi}}{\Sigma_k \Omega_k \cdot e^{-d_{ik}/\psi}} \tag{1}$$

where $\Sigma_k p(s_i, s_k) = 1$, Ω_j is the size $|s_j|$ of settlement s_j, d_{ij} is the geographical distance (i.e., Euclidean distance $(\Delta x^2 + \Delta y^2)^{1/2}$) between the two settlements s_i and s_j, and ψ is a tunable parameter. The ψ parameter can be used to amplify or reduce global mobility; we use a fixed $\psi = 0.2$ in this study, translating to the reduced mobility seen throughout the COVID-19 period (2020–2021). For a full definition of the geo-spatial population model (GPM), which is beyond the goal of our current paper, please refer to our previous contribution [28].

2.2. The SIR-V epidemic model

The proposed epidemic model is summarized in Figure 1 which defines the four states and particular transition rates. Any individual can be in one of the four states: susceptible (S), infected (I), recovered (R) or vaccinated (V). The transition $S \rightarrow I \rightarrow R$ is determined by the classic (normal) infection rate λ_n, and recovery rate μ, respectively. For these transition rates we chose the values $\lambda_n = 0.06$ and $\mu = 0.02$, supported by recent studies which measured an $R_0 = \lambda_n/\mu = 3.3 \pm 1.4$ for COVID-19 [1].

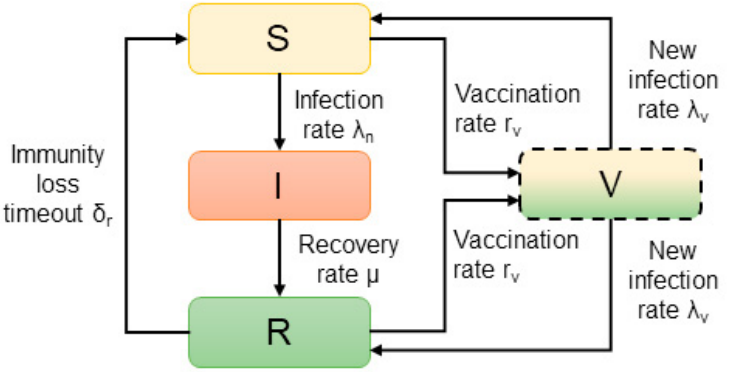

Fig. 1. Overview of our modified SIR epidemic model into a SIR-V model with the following states: susceptible (S), infected (I), recovered (R), vaccinated (V), and specific transmission rates: normal infection rate λ_n, infection rate for vaccinated individuals λ_v, recovery rate μ, vaccination rate r_v, and average timeout for patient relapse δ_r. We consider V a transitory state (hence the dotted contour) since all S/R individuals undergoing vaccination return to their previous S/R state, with the new (lower) infection rate.

Unlike the classic SIR model, we do not model R as a final state for individuals. Given the relatively short immunity to the SARS-CoV-2 virus, all individuals in R will eventual transition back to S after a relapse (timeout) period δ_r. The relapse period for any recovered individual is uniformly chosen between of 3–6 months (i.e., 90–180 iterations), supported by recent estimates of COVID-19 immunity [34] (3 months), [14] (4–5 months), and [37] (6 months).

Also, any susceptible and recovered individuals can undergo vaccination with a rate of r_v (estimated for a 5 year period). For simplicity, we interpret r_v as a global "successful" vaccination rate, not considering the different types of vaccines currently available. From r_v, a daily vaccination rate d_v is computed as $d_v = r_v/5/365$. Thus, a proportion d_v of randomly chosen, non-infected and non-vaccinated individuals transition to the V state every iteration (day). However, this state is transitory, as it simply alters the rate at which nodes will eventually infect and become infected by others. All nodes in V are marked in such a way that their new infection rate becomes λ_v. Vaccination performance is known to vary between 60-95% (based on existing products), however, we use $\lambda_r = 0.25 \cdot \lambda_n$, supported by recent research findings, published in The Lancet, that the reduction in COVID-19 cases dropped by 75% (down to one quarter) compared to non-vaccinated individuals [2].

Overall, our proposed SIR-V model implies a continuous transition of nodes between states $S \rightarrow I \rightarrow R \ldots S$, defined by the relapse timeout δ_r, and the reduction of λ_n to λ_v (used both for infecting and being infected) after each node is vaccinated.

2.3. Geo-spatial and infections datasets

We run GPM at country level, i.e., modeling all settlements inside a chosen country. As such, the number of settlements (and the total simulation population $\Omega = \sum_i \Omega_i$, are defined by a chosen geographical area A, limited by a country's borders. Furthermore, the position (x, y) and size Ω_i of settlements s_i are defined in accordance to the Global Rural-Urban Mapping Project (GRUMP v1) curated by the Center for International Earth Science Information Network (CIESIN), Columbia University [35]. Since the project is still evolving, it is missing some data for various regions of the world. Nevertheless, we choose to model three countries, representative in terms of population density (i.e., which in turn influences the amount of human mobility). In this paper we run a set of experiments on models of Romania, Germany and South Korea. These countries were chosen because of their increasing population densities, as detailed in Table 1, which summarizes the demographic data of each used country model. The focus is to show how population and density play a role in the epidemic dynamics.

Table 1. Country models used in this study, detailing their population density, the real country size (as defined by the GRUMP dataset), the simulation population (used by GPM), and the number of settlements considered in GPM.

Country	Density (pop/km^2)	Real size (GRUMP)	Simulation size (GPM)	Settlements
Romania	81	15.35M	15,357	864
Germany	235	53.31M	53,316	1132
South Korea	512	38.72M	38,722	150

We note that, in order to speed-up the simulation, without loosing notable predictive accuracy [28], we reduce the modeled population Ω uniformly, from reach settlement, by a factor of $\times 1000$ (see column "Simulation size (GPM)" in Table 1). To keep the same population density, we also reduce the size of the total area A by the same $\times 1000$ factor. Experiments show that, as long as the density ($=\Omega/A$) is kept constant, by reducing both Ω and A, the dynamics of the modeled epidemic maintain the same characteristics.

In order to compare our computer simulations output with real epidemic data, we use a recent snapshot of the JHU CSSE COVID-19 dataset, that is being curated by the Center for Systems Science and Engineering (CSSE) at Johns Hopkins University [10]. This comprehensive dataset contains time series information on daily accumulated confirmed Coronavirus cases worldwide. From these numbers we express the absolute daily number of cases, as the difference between each two consecutive days. Also, we estimate the number of infected individuals in a country, for any day d, as the sum of daily cases over the two weeks prior to d (i.e., the sum of daily cases from $d - 13$ to d). This simplification of the estimation of total infected cases is [21].

3. Results

In this section we present the summary of numerical simulations on three country models, with population structure and mobility defined by GPM (see Table 1 for details), and epidemic dynamics according to the proposed SIR-V model (see Figure 1 for details). Our goal is to provide a qualitative assessment of the performance of vaccination strategies. As such, we try to understand how the proportions of infected and recovered individuals (normalized by country population, and expressed in % for convenience) vary based on an increasing vaccination rate $r_v = 0, 0, 1 \ldots 0.9, 1$.

All simulations run for a fixed duration of $t = 2000$ iterations (i.e., days), with vaccination beginning after one year ($t = 365$), as is the case of COVID-19, offering a 5-year post-vaccination overview of the epidemic. For simplicity, we note that the geo-spatial data and the population model do not evolve during this time.

Figure 2a shows the dynamics of COVID-19 using real data from [10] in Romania, measured by the total infected proportion, estimated from the daily number of cases. Here we notice three irregular waves ($w_1 - w_3$) occurring at non-deterministic moments in time. A similar dynamic characteristic is observed in Figure 2b (red dotted area) where the simulated dynamics for Romania (blue) are very similar. Additionally, Figure 2b also plots simulation dynamics for Germany (orange) and South Korea (green). The simulation scenario employs a moderate vaccination rate of $r_v = 0.3$. We notice high variability in the early stages of the simulation ($t = 0 - 400$), that suggest an association with the population density. Indeed, South Korea did adopt early isolation strategies, so it did not have the same infection spike as depicted in Figure 2b (green). After $\approx$ 400 days, the infected proportion has a declining convergent trend, regardless of country density. The same conclusion can be drawn from the inset of Figure 2b, where the recovered proportion converges for all countries.

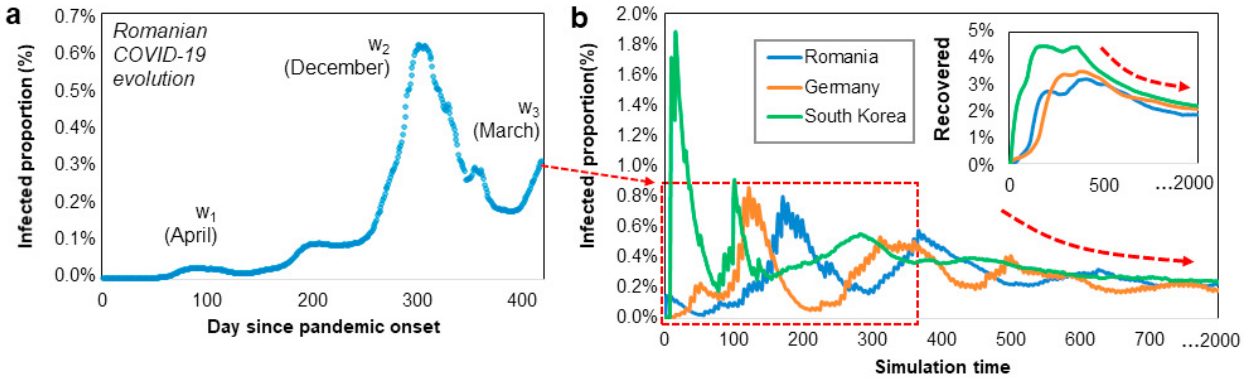

Fig. 2. (a) Heterogeneous characteristic of COVID-19 spreading (in Romania) from outbreak onset to March 2021. The dynamics shows three waves ($w_1 - w_3$) occurring at non-deterministic times and of variable amplitude. (b) Simulation results for a vaccination rate of $r_v = 0.3$, using GPM for three country models with distinct population densities (Romania-81; Germany-235; S.Korea-512 inhabitants/km^2). The infected proportion during the first year of simulation displays high variability, but converges after $\approx$ 2 years to a slowly declining trend, regardless of country density. The same observation is valid for the recovered proportion depicted in the inset of panel (b). Real data in panel (a) are depicted starting from the beginning of 2020, while simulation data in (b) start from the first actual cases ($\approx$ 3 months later), thus explaining the slight temporal shift on the OX-axis.

In Figure 3 we depict the impact of vaccinating the general population by comparing three strategies: no vaccination ($r_v = 0$), moderate vaccination ($r_v = 0.3$), and strong vaccination ($r_v = 0.9$) over a 5-year period (Jan/2021–Dec/2025). It is obvious that the effects of the pre-vaccination period cannot be undone, but once vaccination starts ($t \geq 365$), it becomes clear that both strategies (blue, green) reduce the number of infected individuals noticeably. During the early vaccination period (2021–2022), infection waves will still be probable for the moderate strategy ($r_v = 0.3$), while the stronger strategy seems to dampen these waves better. During the moderate-term period (2023–2025), we notice that both vaccination strategies converge similarly, and keep the infected ratio much smaller than without any vaccination. Specifically, our SIR-V model pinpoints a drop in the infected proportion from $> 0.4\%$ (orange line) in case of no vaccination, down to $< 0.2\%$ infected in case of any of the two other vaccination strategies (green, blue lines).

Next, we focus on detailing the impact of a more granular vaccination rate r_v. Figure 4a depicts a snapshot from $t = 1000 - 2000$ (roughly Jan/2023–Dec/2025), after the infected proportion has dampened for most vaccination

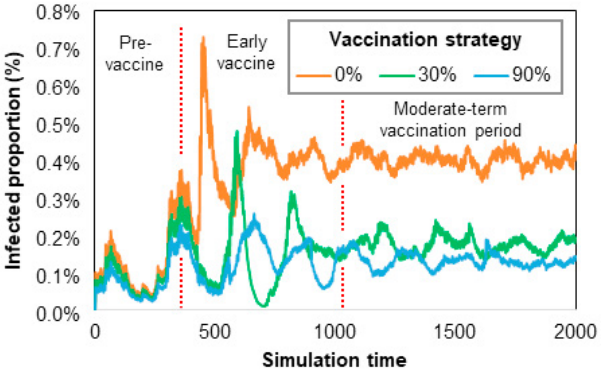

Fig. 3. The impact of a moderate vaccination strategy (30%, green line), a strong vaccination strategy (90%, blue line) versus no vaccination in the population (0%, orange line). The first part (pre-vaccine) of the simulation period is more unpredictable due to the heterogeneity of population structure and mobility (considered by our GPM model). After $\approx t > 400$ we notice a significant impact of both vaccination strategies – larger waves are avoided, and the dynamics converges towards a smaller overall infected proportion of $< 0.2\%$, instead of $> 0.4\%$ visible for the no vaccination strategy. Nevertheless, our simulation shows no significant difference between the 30% and 90% strategies given a moderate temporal perspective (2-5 years).

strategies, which suggest no more visible epidemic waves. Without a vaccination policy ($r_v = 0$, dark blue line), the infected count would reach a high, pseudo-constant proportion of 0.4–0.5%, comparable to a permanent infection wave. To put the simulation results into perspective, in early 2021, Romania saw a second wave ending and a third wave unfolding with about 0.3–0.5% of the population infected with SARS-CoV-2.

The "weakest" vaccination strategy, depicted in Figure 4a, is $r_v = 0.2$ (orange line) and converges slowly towards the dynamical characteristic of the other stronger strategies ($r_v \geq 0.4$). That is, all other strategies with $r_v \geq 0.4$ produce similar infection dynamics. We note that the pandemic is not eradicated over the 5-year simulation window, but it remains as a permanent viral outbreak without significant waves. We believe this happens because the vaccination does not render total immunity (rather 75% reduction in ineffectiveness), and because the global vaccination is most likely going to be a very slow process.

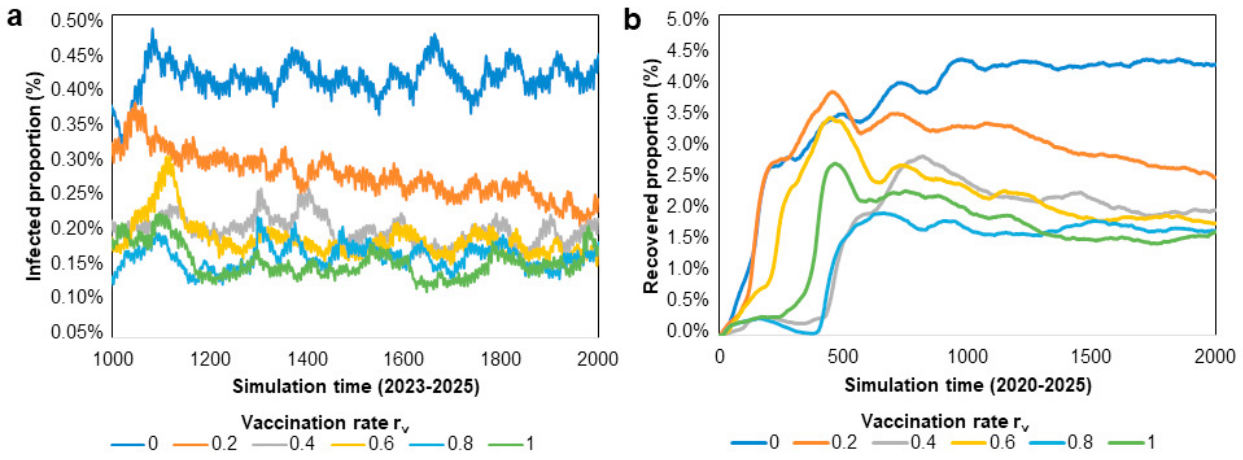

Fig. 4. (a) Estimation of the infected proportion for variable vaccination rates $r_v \in \{0, 0.2, 0.4, 0.6, 0.8, 1\}$. The result snapshot is focused on the second half of the simulation period, i.e., $t = 1000 - 2000$ which roughly translates to the 3-year interval from Jan/2023 to Dec/2025. We observe that all vaccination rates converge towards an infected proportion of 0.15–0.2%, but a rate of $r_v \geq 0.4$ yields better results than $r_v = 0.2$ in the earlier stages (2022-2024). (b) Estimation of the recovered proportion for the same variable vaccination rates. Results reinforce the idea that a $r_v = 0.2$ is non-ideal (too small), but as $r_v \geq 0.4$, we obtain similar mid-term results. Note that the set of recovered individuals decreases since we model a patient relapse (back to susceptible) after an average timeout period δ_r.

Supporting the same observations is Figure 4b, which depicts the recovered proportion for all vaccination rates, during the whole simulation period $t = 0 - 2000$. Note that the recovered population does not grow constantly, as in the case of SIR, because our SIR-V epidemic model implies a continuous relapse from $R \rightarrow S$. Plotting the recovered proportion gives clearer insights into the efficacy of vaccination strategies. To that end, by focusing on the early to mid vaccination period ($t > 400$), we can consider only the rates $r_v \geq 0.4$ as effective, in terms of keeping the recovered proportion below 3% at any time. When $r_v = 0.2$ (orange line) we measure a duration of almost two years until the recovered proportion drops permanently below 3%. For the reference scenario, without vaccination (dark blue line), the recovered proportion converges to an alarming 4.5% of the total population.

Our simulations show irregular, non-deterministic dynamics in the early part of the vaccination period ($t \approx 500 - 1000$), a characteristic that has been so far confirmed during the 2020–2021 COVID-19 pandemic. In this early post-vaccination period, we observe spikes in infection ratio which tend to disappear towards the moderate-term period. To better quantify the distinct dynamics of these two periods, and also relate them to the vaccination rate r_v, we provide Figure 5. As such, we measure the maximum (Max) value of the infected and recovered waves, as well as the final (End) value of convergence (i.e., average value of infected and recovered during the period $t = 1500 - 2000$).

Figure 5a suggests that, as the vaccination rate r_v increases, the difference between the maximum and end values of infected increases from about ×2 to ×4. Also, we notice that starting with $r_v \geq 0.2$ the amplitude of the maximum infection wave (orange line) remains the same. Nevertheless, the end value of the infection proportion (blue line) decreases steadily as r_v increases, up to $r_v \approx 0.6$. Since we address a long term epidemic, we should strive for a stronger vaccination policy.

Figure 5b suggests that the proportion of recovered individuals is reduced more significantly starting from $r_v \geq 0.5$. Thus, the difference between the maximum recovered and end value of recovered proportions increases to ×1.8 when a stronger vaccination is adopted.

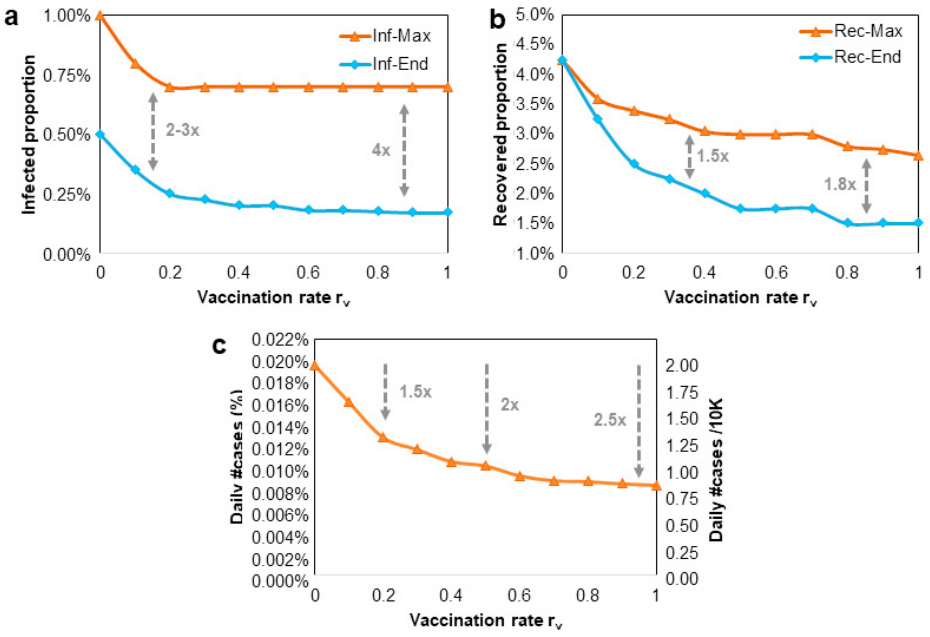

Fig. 5. The relationship between three relevant epidemic metrics and the vaccination rate r_v. (a) Maximum (peak during whole simulation period) and End (average convergence value when $t \rightarrow 2000$) proportions of infected individuals. (b) Maximum and End proportions of recovered individuals. Vertical arrows suggest a multiplicative reduction from Max to End values. (c) Estimated daily number of cases (% and per 10K individuals) as the vaccination rate is increased. Vertical arrows suggest a multiplicative reduction compared to no vaccination ($r_v = 0$).

Finally, we depict in Figure 5c the daily number of cases, as influenced by the vaccination rate r_v. We notice that the number of cases drops with r_v. This rate is non-linear, but may be fitted by a logarithmic downward trend. Based on

the strength of the vaccination strategy, we may reduce the daily number of cases by ×1.5 up to ×2.5, which translates into (partial to total) dampening the effect of COVID-19 waves.

All the results depicted in Figures 3-5 are based on 100 repeated computer simulations. We did not include additional error bars or confidence intervals in order not to over-complicate the visualizations, and because the convergence results ($t > 1000$) are highly stable in all presented scenarios.

4. Conclusions

Current scientific efforts to predict and control the COVID-19 pandemic represent global-scale efforts and include the customization of available SIR/SEIR models [15, 18, 30, 22]. However, the predominant usage of underlying homogeneous mixing models, which adopt a single population scale [6, 27, 5, 4, 12], impede the reproduction of meaningful characteristics of real-world epidemic outbreaks. Conversely, Network Science inspired approaches can contribute to better modeling of complex systems in general [23, 31, 32], by considering network topology, community structure, and human mobility patterns [24, 25, 26].

This paper proposes an original intelligent information system which provides a qualitative assessment of the performance of vaccination strategies, in the COVID-19 context, summarizing an overview over the moderate-term period 2021–2025. To replicate real-world conditions, we adopt a heterogeneous population model with mobility, based on creating stochastic blocks, according to the size and geographical location of each settlement inside a chosen country [28]. Also, we propose a SIR-V epidemic model, which, unlike the classic SIR, considers patient relapse from $R \rightarrow S$ based on a relapse timeout δ_r in accordance to recent epidemiological studies [34, 14, 37]. Also, SIR-V implements individual vaccination with a variable rate r_v. Nevertheless, in accordance to recent studies [2], vaccination does not offer long term immunity, rather it reduces the probability of becoming infected and the infectious rate in case of infection. This new rate λ_v is updated for all vaccinated individuals. Finally, we only start the vaccination strategy after a timeout of $t = 365$ iterations (1 year), in compliance with the real-world situation.

We employ computer simulations of epidemic outbreaks over a $\approx$ 6-year period ($t = 2000$ iterations/days) at country level for GPM models of Romania, Germany and South Korea. The experiments reveal a high variability in the early stages of the simulation ($t = 0 - 400$), that suggest a correlation with the population density. Namely, denser countries have a higher chance of developing larger initial waves in case no strict isolation is imposed. After the first simulation year, and after vaccination starts ($t > 400$), the proportion of infected individuals has a declining convergent trend, regardless of country density. By testing different vaccination rates $r_v = 0 - 1$ we find that during the early vaccination period (roughly 2021–2022), waves of infection are still probable for moderate vaccination strategies ($r_v \leq 0.3$), while stronger strategies manage to dampen subsequent waves better. During the moderate-term period (roughly 2023-2025), most vaccination strategies ($r_v \geq 0.2$) converge similarly, and keep the infected ratio much smaller than without any vaccination.

In favor of adopting vaccination strategies worldwide, our results suggest that, without a vaccination policy ($r_v = 0$), the infected count would maintain a high, pseudo-constant proportion of 0.4–0.5%, that is comparable to a permanent infection wave. Weaker vaccination, at a rate of just $r_v = 0.2 - 0.4$ (i.e., 20-40% of the total population, over 5 years), will still converge slowly towards the dynamical characteristics of the other stronger strategies. All vaccination strategies with $r_v \geq 0.4$ produce similar infection dynamics by maintaining the infected proportion below 0.2%, compared to 0.4–0.5%, in case of no vaccination. We observe that the pandemic is not eradicated over the 5-year simulation window, but remains as a permanent viral outbreak without significant waves (i.e., in case we implement vaccination). We believe this happens because the current vaccination is not able to offer total immunity, because of the inevitable patient relapse, and because the global vaccination is a very slow process. Finally, we quantify the reduction in daily number of cases to drop by ×1.5 up to ×2.5 for vaccination rates $r_v = 0.2 - 1$. In general, the results offered by our realistic epidemic model encourage stronger (i.e., faster, at $r_v \geq 0.4$) vaccination strategies to be adopted worldwide.

Indeed, our study is still limited by our full understanding of the COVID-19 pandemic, on the performance of available vaccines, on the evolving new viral strains, and on in-depth global contact tracing data. As a future direction, we consider the update of the SIR-V model with new epidemiological findings, addition of an E (exposed) state, and heterogeneous (regional) vaccination policies. Also, real and simulated epidemic dynamics, based on time series data, could be further compared using a multi-variable similarity metric such as the statistical fidelity [29]. Overall, we

believe that our study, based on the synergy of the original GPM and SIR-V models, represents a timely contribution for tackling the current COVID-19 pandemic and supporting global decision makers.

Acknowledgments

This work was supported by a grant of the Romanian Ministry of Education and Research, CNCS - UEFISCDI, project number PN-III-P1-1.1-PD-2019-0379, within PNCDI III.

Competing interests

The authors declare no competing interests.

References

[1] Alimohamadi, Y., Taghdir, M., Sepandi, M., 2020. Estimate of the basic reproduction number for COVID-19: a systematic review and meta-analysis. Journal of Preventive Medicine and Public Health 53, 151.
[2] Amit, S., Regev-Yochay, G., Afek, A., Kreiss, Y., Leshem, E., 2021. Early rate reductions of SARS-CoV-2 infection and COVID-19 in bnt162b2 vaccine recipients. The Lancet 397, 875–877.
[3] Anderson, R.M., May, R.M., Anderson, B., 1992. Infectious diseases of humans: dynamics and control. volume 28. Wiley Online Library.
[4] Arenas, A., Cota, W., Gomez-Gardenes, J., Gómez, S., Granell, C., Matamalas, J.T., Soriano-Panos, D., Steinegger, B., 2020. A mathematical model for the spatiotemporal epidemic spreading of COVID-19. MedRxiv .
[5] Atkeson, A., 2020. What will be the economic impact of COVID-19 in the us? rough estimates of disease scenarios. Technical Report. Nat. Bureau of Economic Research.
[6] Block, P., Hoffman, M., Raabe, I.J., Dowd, J.B., Rahal, C., Kashyap, R., Mills, M.C., 2020. Social network-based distancing strategies to flatten the COVID-19 curve in a post-lockdown world. Nature Human Behaviour , 1–9.
[7] Chen, J., Zhang, H., Guan, Z.H., Li, T., 2012. Epidemic spreading on networks with overlapping community structure. Physica A: Statistical Mechanics and its Applications 391, 1848–1854.
[8] Cohen, J., Kupferschmidt, K., 2020. Countries test tactics in 'war'against COVID-19.
[9] Diaz, P., Constantine, P., Kalmbach, K., Jones, E., Pankavich, S., 2018. A modified seir model for the spread of ebola in western africa and metrics for resource allocation. Applied Mathematics and Computation 324, 141–155.
[10] Dong, E., Du, H., Gardner, L., 2020. An interactive web-based dashboard to track COVID-19 in real time. The Lancet infectious diseases 20, 533–534.
[11] Dye, C., Gay, N., 2003. Modeling the sars epidemic. Science 300, 1884–1885.
[12] Ferguson, N.M., Cummings, D.A., Fraser, C., Cajka, J.C., Cooley, P.C., Burke, D.S., 2006. Strategies for mitigating an influenza pandemic. Nature 442, 448–452.
[13] Ferrari, M.J., Grais, R.F., Bharti, N., Conlan, A.J., Bjørnstad, O.N., Wolfson, L.J., Guerin, P.J., Djibo, A., Grenfell, B.T., 2008. The dynamics of measles in sub-saharan africa. Nature 451, 679–684.
[14] Gudbjartsson, D.F., Norddahl, G.L., Melsted, P., Gunnarsdottir, K., Holm, H., Eythorsson, E., Arnthorsson, A.O., Helgason, D., Bjarnadottir, K., Ingvarsson, R.F., et al., 2020. Humoral immune response to SARS-CoV-2 in iceland. New England Journal of Medicine 383, 1724–1734.
[15] Hellewell, J., Abbott, S., et al., 2020. Feasibility of controlling COVID-19 outbreaks by isolation of cases and contacts. The Lancet Global Health .
[16] Holland, P.W., Laskey, K.B., Leinhardt, S., 1983. Stochastic blockmodels: First steps. Social networks 5, 109–137.
[17] Koo, J., Cook, A., Park, M., et al., 2020. Interventions to mitigate early spread of COVID-19 in singapore: a modelling study. Lancet Infect Dis. doi:10.1016/S1473-3099(20)30162-6.
[18] Kucharski, A.J., Russell, T.W., et al., 2020. Early dynamics of transmission and control of COVID-19: a mathematical modelling study. The Lancet Infectious Diseases .
[19] Kupferschmidt, K., Cohen, J., 2020. China's aggressive measures have slowed the coronavirus. they may not work in other countries. Science. Mar .
[20] McLean, A.R., May, R.M., Pattison, J., Weiss, R.A., et al., 2005. SARS: a case study in emerging infections. Oxford University Press.
[21] Noh, J., Danuser, G., 2021. Estimation of the fraction of COVID-19 infected people in us states and countries worldwide. PloS one 16, e0246772.
[22] Prem, K., Liu, Y., Russell, T.W., Kucharski, A.J., Eggo, R.M., Davies, N., Flasche, S., Clifford, S., Pearson, C.A., Munday, J.D., et al., 2020. The effect of control strategies to reduce social mixing on outcomes of the COVID-19 epidemic in wuhan, china: a modelling study. The Lancet Public Health .
[23] Salathé, M., Jones, J.H., 2010. Dynamics and control of diseases in networks with community structure. PLoS Comput Biol 6, e1000736.
[24] Salathé, M., Kazandjieva, M., Lee, J.W., Levis, P., Feldman, M.W., Jones, J.H., 2010. A high-resolution human contact network for infectious disease transmission. Proceedings of the National Academy of Sciences 107, 22020–22025.

[25] Shang, J., Liu, L., Li, X., Xie, F., Wu, C., 2015. Epidemic spreading on complex networks with overlapping and non-overlapping community structure. Physica A: Statistical Mechanics and its Applications 419, 171–182.
[26] Stegehuis, C., Van Der Hofstad, R., Van Leeuwaarden, J.S., 2016. Epidemic spreading on complex networks with community structures. Scientific reports 6, 1–7.
[27] Thunström, L., Newbold, S.C., Finnoff, D., Ashworth, M., Shogren, J.F., 2020. The benefits and costs of using social distancing to flatten the curve for COVID-19. Journal of Benefit-Cost Analysis , 1–27.
[28] Topîrceanu, A., 2020. Analyzing the impact of geo-spatial organization of real-world communities on epidemic spreading dynamics, in: International Conference on Complex Networks and Their Applications, Springer. pp. 345–356.
[29] Topirceanu, A., Udrescu, M., 2017. Statistical fidelity: a tool to quantify the similarity between multi-variable entities with application in complex networks. International Journal of Computer Mathematics 94, 1787–1805.
[30] Topirceanu, A., Udrescu, M., Marculescu, R., 2020. Centralized and decentralized isolation strategies and their impact on the COVID-19 pandemic dynamics. arXiv preprint arXiv:2004.04222 .
[31] Topîrceanu, A., Udrescu, M., Udrescu, L., Ardelean, C., Dan, R., Reisz, D., Mihaicuta, S., 2018. Sas score: Targeting high-specificity for efficient population-wide monitoring of obstructive sleep apnea. PloS one 13, e0202042.
[32] Topirceanu, A., Udrescu, M., Vladutiu, M., 2014. Genetically optimized realistic social network topology inspired by facebook, in: Online Social Media Analysis and Visualization. Springer, pp. 163–179.
[33] Wallinga, J., Teunis, P., 2004. Different epidemic curves for severe acute respiratory syndrome reveal similar impacts of control measures. American Journal of epidemiology 160, 509–516.
[34] Ward, H., Cooke, G., Atchison, C.J., Whitaker, M., Elliott, J., Moshe, M., Brown, J.C., Flower, B., Daunt, A., Ainslie, K.E., et al., 2020. Declining prevalence of antibody positivity to SARS-CoV-2: a community study of 365,000 adults. MedRxiv .
[35] Warszawski, L., Frieler, K., et al., 2017. Center for international earth science information network—ciesin—columbia university. gridded population of the world, version 4 (gpwv4). nasa socioeconomic data and applications center (sedac). doi: 10. 7927/h4np22dq. Atlas of Environmental Risks Facing China Under Climate Change , 228.
[36] Watts, D.J., Muhamad, R., Medina, D.C., Dodds, P.S., 2005. Multiscale, resurgent epidemics in a hierarchical metapopulation model. Proceedings of the National Academy of Sciences 102, 11157–11162.
[37] Zuo, J., Dowell, A., Pearce, H., Verma, K., Long, H., Begum, J., Aiano, F., Amin-Chowdhury, Z., Hallis, B., Stapley, L., et al., 2020. Robust SARS-CoV-2-specific t-cell immunity is maintained at 6 months following primary infection. BioRxiv .